CONF-860605--24

THE FINE SCALE MICROSTRUCTURE IN CAST AND AGED DUPLEX STAINLESS STEELS INVESTIGATED BY SMALL ANGLE NEUTRON SCATTERING*

J. E. Epperson, J. S. Lin** and S. Spooner**
Materials Science and Technology Division
Argonne National Laboratory
Argonne, Illinois 60439

**Solid State Division
Oak Ridge National Laboratory
Oak Ridge, Tennessee 37831

CONF-860605--24

DE86 014499

February 1986

DISCLAIMER

*Work supported by the U.S. Department of Energy, BES-Materials Sciences, under Contract W-31-109-Eng-38.

Submitted to the Thirteenth International Symposium on Effects of Radiation on Materials, June 23-25, 1986, held in Seattle, Washington.

THE FINE SCALE MICROSTRUCTURE IN CAST AND AGED DUPLEX STAINLESS STEELS INVESTIGATED BY SMALL ANGLE NEUTRON SCATTERING*

J. E. Epperson, J. S. Lin** and S. Spooner**
Materials Science and Technology Division
Argonne National Laboratory
Argonne, Illinois 60439

**Solid State Division
Oak Ridge National Laboratory
Oak Ridge, Tennessee 37831

FINAL

February 1986

*Work supported by the U.S. Department of Energy, BES-Materials Sciences, under Contract W-31-109-Eng-38.

Submitted to the Thirteenth International Symposium on Effects of Radiation on Materials, June 23-25, 1986, held in Seattle, Washington.

THE FINE SCALE MICROSTRUCTURE IN CAST AND AGED DUPLEX STAINLESS STEELS INVESTIGATED BY SMALL ANGLE NEUTRON SCATTERING*

J. E. Epperson, J. S. Lin** and S. Spooner**
Materials Science and Technology Division
Argonne National Laboratory
Argonne, Illinois 60439

**Solid State Division
Oak Ridge National Laboratory
Oak Ridge, Tennessee 37831

Abstract

Small angle neutron scattering (SANS) allows clustering phenomena to be studied in systems for which the constituent atoms do not differ greatly in atomic number. This investigation used SANS to characterize the fine scale microstructure in two cast and aged duplex stainless steels; aging times extended up to eight years. The steels differed in ferrite content by about a factor of two. The scattering at lowest q was dominated by magnetic scattering effects associated with the ferrite phase. In the range $0.025 \lesssim q \lesssim 0.2 \text{Å}^{-1}$, additional scattering due to a precipitating phase rich in Ni and Si was observed. This scattering was rather intense and revealed a volume fraction of precipitate, in the ferrite, estimated to be 12-18 percent after long time aging. After about 70,000 hours at 400°C, there were about 10^{18} precipitate particles per cm^3 some 50Å in mean diameter, and they were distributed in a non-random manner; i.e., spatially, short-range-ordered. This investigation suggests that after aging some 70,000 hours at 400°C, the precipitate in the ferrite phase is undergoing Ostwald ripening. The present data are insufficient to indicate at what time this ripening process began.

*Work supported by the U.S. Department of Energy, BES-Materials Sciences, under Contract W-31-109-Eng-38.

THE FINE SCALE MICROSTRUCTURE IN CAST AND AGED DUPLEX STAINLESS STEELS INVESTIGATED BY SMALL ANGLE NEUTRON SCATTERING*

J. E. Epperson, J. S. Lin** and S. Spooner**
Materials Science and Technology Division
Argonne National Laboratory
Argonne, Illinois 60439

**Solid State Division
Oak Ridge National Laboratory
Oak Ridge, Tennessee 37831

I. Setting of the Problem

Because of the desirable properties imparted by the ferrite phase, cast duplex stainless steels have found wide usage in the nuclear industry for fabrication of such essential components as pipes and pumps. Among these attributes are improved soundness of the castings, increased tensile strength, improved weldability and resistance to stress corrosion cracking. However, not all the effects due to the presence of ferrite are positive.

In addition to the major constituents, commercial steels invariably contain a range of minor constituents, and known to form are various carbides, Co-rich sigma and chi phases and a Cr-rich bcc phase denoted as α'. The σ-phase forms at temperatures above about 650°C, the χ-phase in the range from about 500 to 650°C and the α' somewhat below 500°C as shown in Fig. 1 from Solomon and Devine.[1] Generally, these minor phases cause the alloy to become quite brittle with respect to shock loading,[2] a disconcerting problem in their nuclear power industry applications. However, the low cycle fatigue properties and fatigue crack propagation rates are reported not to be appreciably influenced by annealing at temperatures from 300 to about 400°C.[3] The most extensively investigated of these reactions is surely the α'

*Work supported by the U.S. Department of Energy, BES-Materials Sciences, under Contract W-31-109-Eng-38.

formation, which is most rapid at 475°C. The resulting effect on the alloy properties has led to the term "475° embrittlement". It is currently accepted that the 475°C embrittlement is due to the presence of coherent precipitates which in turn are due to the existence of a miscibility gap in the phase diagram at a temperature below that required for σ-phase formation.[4,5] Fine precipitates about 200 Å in diameter and containing some 60-80 percent Cr have been extracted from an Fe-28.5 wt.% Cr alloy aged at 475°C for up to 3 years by Fisher, Dulis and Carroll.[6] This conclusion was confirmed by Marcinkowski, Fisher and Szirmae[7] by transmission electron microscopy (TEM) without having to resort to extraction techniques. Reversion of the α'-phase can be brought about by heating to above about 550°C.

Until recently, the embrittlement of ferritic steels at the operating temperature of light water nuclear power reactors (288-316°C) was attributed to the presence of fine α' precipitates. Analysis of the aging data from the 300-400°C range for cast duplex stainless by Trautwein and Gysel[8] yielded an apparent activation energy for the onset of embrittlement of 24,000 cal/mole. This result is confusing, for single-solute-atom bulk diffusion would predict a value of 54,900 cal/mole, and this has led to a reconsideration of the microstructural cause of the changes in properties due to low temperature aging. On the basis of this result, it has been suggested[9] that the α' precipitation is not formed by nucleation and growth but by some continuous process or that some process other than α' precipitation is responsible for the low temperature embrittlement.

The microstructure produced by long time aging at low temperature has been investigated by TEM by Chopra and Ayrault.[9] No precipitation was observed in an unaged, cast duplex stainless steel. The micrographs of the cast and aged duplex stainless steel samples did not reveal the mottled

bright-field TEM images which are often taken as the signature of the α' precipitates. Rather, the duplex steel annealed for 66,650 hours at 400°C (corresponding to our SS#4 in Table 2) revealed a profusion of precipitates in the ferrite phase, but no precipitates were observed in this alloy after annealing for only 10,000 hours at 400°C (corresponding to SS#8 in Table 2). These precipitates were reported to be fcc and about 50Å in diameter (those homogeneously nucleated) with a unit cell parameter some 3.95 times that of the ferrite matrix and to be similar to what Chopra and Ayrault have termed "$M_{23}C_6$-like" precipitates. Their preliminary energy-dispersive x-ray analysis indicated enrichment of the precipitates in Ni and Si, suggesting that the $M_{23}C_6$-like phase may be the S-phase* reported by Brown and Allsop.[11] Another type of precipitate with low volume fraction was observed to form on dislocations. This latter was the only precipitation observed for heat 280 annealed 70,000 hours at 300°C, but $M_{23}C_6$-like precipitates also were seen in abundance in heat 278 given the same heat treatment.

Because the annealing temperatures for this series of duplex stainless steel samples from the George Fisher Co. approach so closely that of the operating temperature for the light water reactors in which such alloys are in use, the TEM work is being extended by Chopra and Chung.[10] This work has confirmed the observations of Chopra and Ayrault, and additional phases in small volume fractions have been observed. At last count, the number of low temperature phases stands at seven,[12] including α'; however, several of these are present in extremely minute concentrations.

Because of the complementarity of small angle neutron scattering (SANS) and transmission electron microscopy techniques, and particularly in view of

*Brown and Allsop[11] give the composition of the S-phase as (in wt.%): 13.4 Si - 52.3 Ni - 8.4 Mn - 15.7 Cr - 10.2 Fe.

the sensitivity of SAS measurements to very small particles, the present SANS investigation was deemed worthwhile as a means of obtaining additional information about the fine scale microstructure in these cast and aged duplex stainless steels.

II. Sample Preparation and History

The samples used in this investigation were obtained by J. B. Darby, Jr.[13] from George Fisher, Ltd. in Switzerland. The overall compositions of the two commercial grade alloys are given in Table 1. The alloys had been cast in bulk form and machined to the dimensions required for Charpy impact testing; that is, rectangular bars approximately 1 x 1 cm^2 in cross section. We actually had one half of such broken Charpy impact samples from the batch of samples used by Trautwein and Gysel[8] in their study of the long time aging behavior of these steels.

The solidification process resulted in the formation of a two-phase microstructure consisting of austenite and ferrite, hence the common generic designation of these materials as cast duplex stainless steels. The proportions of these two phases are indicated in Table 1. The samples investigated here had been annealed in the laboratory at 300°, 350° or 400°C for times ranging from 3,000 h to 70,000 h (7.99 years) as shown in Table 2.

Local preparation of the samples consisted only of grinding the sample sides so as to yield parallel faces free of oxide films, etc. and to polish the resulting faces mechanically through the lapping wheel.

III. Relevant Scattering Theory

Conventional neutron scattering[14] arises from the interaction between the projectile neutron and the nucleus of the target atom. In addition, if an atom has unpaired electrons, it may scatter neutrons due to an interaction between the resulting magnetic moment of the atom and that of the neutron.

One component of the nuclear scattering is measured by the effective cross section the nucleus presents to the incoming beam of neutrons. This is the potential scattering and is found to increase proportional to the cube root of the atomic mass of the nucleus. A process known as resonance scattering is superimposed on the potential scattering due to the nuclear size. It is convenient to think of the incident neutron and target atom as forming a compound nucleus, and, depending on the energy levels of this compound state, resonance scattering may take place. The amplitude of the resonance scattering may be of the same or opposite sign to that of the potential scattering, leading to an increase or decrease in the total scattering amplitude; in exceptional cases the resulting total coherent scattering amplitude may be negative. Resonance scattering varies in a non-regular manner with atomic number, and can even be quite different for different isotopes of a given atom. It is this property which often makes it possible to investigate neighboring atoms in the periodic table with neutrons and hence makes neutron-small-angle-scattering a particularly valuable complementary technique to x-ray scattering and to TEM, studies of steels being a good example of this usage.

Coherent small angle scattering has its origin in fluctuations in the scattering length density extending upwards from a few times the projectile wavelength being used in the experiment. SANS is practically independent of

the local atomic order within the fluctuations but is determined by the size, external form, number density and distribution of particles.

For a system that yields both nuclear and magnetic small angle scattering, the differential elastic scattering cross section of an unpolarized beam from a single magnetic particle is given by the sum of the nuclear and magnetic contributions according to[15]

$$\frac{d\sigma}{d\Omega} = \left(\frac{d\sigma}{d\Omega}\right)_{nuc} + \left(\frac{d\sigma}{d\Omega}\right)_{mag}$$
$$= \left| \int \Delta\rho_{nuc}(\vec{r}) e^{i\vec{q}\cdot\vec{r}} d\vec{r} \right|^2 + \left[1 - \left(\frac{\vec{q}\cdot\vec{M}}{|\vec{q}|\,|\vec{M}|}\right)^2\right] \left| \int \Delta\rho_{mag}(\vec{r}) e^{i\vec{q}\cdot\vec{r}} d\vec{r} \right|^2 , \qquad (1)$$

where $|\vec{q}|$ is the magnitude of the scattering vector,

$$q = \frac{4\pi}{\lambda} \sin\theta , \qquad (2)$$

2θ is the scattering angle, λ is the neutron wavelength, $\vec{r}$ is a position vector within the particle, $\Delta\rho_x$ is the appropriate difference in scattering length density, and $\vec{M}$ is the magnetization vector. The term in square brackets in eq. 1 can be written as

$$\sin^2\alpha = 1 - \left(\frac{\vec{q}\cdot\vec{M}}{|\vec{q}|\,|\vec{M}|}\right)^2 , \qquad (3)$$

where α is the angle between the scattering vector and the magnetization direction. Note that if a saturating, external magnetic field is applied during the SANS measurements, the magnetic contribution vanishes when the scattering vector is parallel to the magnetic field direction and that the two contributions add when $\vec{q}$ is normal to $\vec{M}$. This relationship can be

utilized to effect a separation of the nuclear and magnetic components of the scattering and hence permit a more straightforward analysis.

The following discussion will pertain only to the nuclear component of scattering. In the truly small angle limit, the macroscopic scattering cross section for a random assemblage of N_p particles,

$$\frac{d\Sigma}{d\Omega} = n \frac{d\sigma}{d\Omega} , \tag{4}$$

can be adequately represented by the Guinier approximation[16]

$$\frac{d\Sigma(q)}{d\Omega} = \frac{N_p}{V_i} (\Delta\rho)^2 V_p^2 e^{-R_g^2 q^2/3} , \tag{5}$$

where n is the nuclear density, V_i is the irradiated volume of sample, V_p is the volume of a single particle and R_g is the well known Guinier radius of the particle.

The limiting scattering law in the high q region of the SANS profile is given by the Porod approximation[17]

$$\frac{d\Sigma(q)}{d\Omega} = \frac{2\pi}{q^4} (\Delta\rho)^2 \frac{\Delta S}{V_i} , \tag{6}$$

where ΔS is the total interfacial area contained in the irradiated volume. In the real case, this scattering may be superimposed on a nearly constant sample and/or instrument dependent background.

If the macroscopic cross section data are in absolute units (cm^{-1}) and if one knows the composition of the second phase particles, additional information can be derived. For example, the number density of second phase particles is related to the zero-angle scattering by

$$\frac{N_p}{V_i} = \frac{\frac{d\Sigma(0)}{d\Omega}}{(\Delta\rho)^2 V_p^2} \quad . \tag{7}$$

The volume fraction of the second phase is obtained from the integrated SANS according to the relationship

$$\frac{\Delta V}{V_i} = \frac{1}{2\pi^2(\Delta\rho)^2} \int_o^\infty q^2 \frac{d\Sigma}{d\Omega}(q)\, dq. \tag{8}$$

The method outlined above yields only average values for the material parameters; e.g., the Guinier radius. In real metallurgical systems, however, a range of particle sizes is invariably to be expected, and the integral transform method of Brill and Schmidt (BS)[18] is one means of extracting more detailed information for non-interacting spherical particles from the SAS data. According to this procedure, the diameter distribution, $\rho(D)$, is given by

$$\rho(D) = \frac{A}{D^2} \int_o^\infty \left[q^4 \frac{d\Sigma}{d\Omega}(q) - C_4\right] \beta(qD)\, dq \quad , \tag{9}$$

where A is a constant, C_4 is given by

$$C_4 = \lim_{q\to\infty} q^4 \frac{d\Sigma}{d\Omega}(q) \quad , \tag{10}$$

and

$$\beta(qD) = \left[1-8(qD)^{-2}\right] \cos(qD) - \left[4-8(qD)^{-2}\right] \left[\frac{\sin(qD)}{(qD)}\right] \quad . \tag{11}$$

A computer code for carrying out this analysis has been described by Epperson, Loomis and Lin.[19] This BS analysis is performed on the radially averaged SANS data, and the results, in addition to yielding the particle size distribution, provide a useful consistency check on the materials parameters derived in the more conventional manner.

IV. Data Collection and Reduction

The SANS measurements were made at the 30-meter instrument at the National Center for Small Angle Scattering (NCSASR) at Oak Ridge National Laboratory.[20] This choice was dictated by the necessity of having neutrons with sufficiently low energy to avoid contaminating the experiment with multiple Bragg scattering from the crystalline samples.

Neutrons of 4.75Å wavelength were obtained by diffraction from two anti-parallel gangs of pyrolytic graphite monochromator crystals. Appropriately sized circular apertures in Cd plates were used to effect "pinhole" collimation of the monochromatic beam of neutrons. The scattered neutrons were detected with a 64 x 64 cm^2 gas filled (3 atmospheres of ^3He with CCl_4 as the quench gas), position-sensitive proportional counter of the Kopp-Borkowski type.[21] This detector was mounted on rails inside the evacuated flight path, permitting continuous changes in the sample-detector distance from 1.3 to 18.9 meters. In this experiment, sample-detector distances of 2.0, 10.8 and 18.9 meters were used which allowed the q-range from 0.0028 to 0.21$Å^{-1}$ to be sampled, incrementally. For some of the measurements, a 4 kilogauss permanent magnet was mounted on the sample stage and the scattering measured with the stainless steel sample positioned in the gap of the magnet. All measurements were made at room temperature.

The steel samples were polycrystalline and, except when the magnetic field was applied, all the two-dimensional scattering patterns were isotropic. After correcting the observed scattering (normalized according to the monitor count) for variations in the detector sensitivity, dark current absorption in the sample and empty camera background, the cross section data were radially averaged to yield one-dimensinal histograms of I(q) vs q. Except for the 2-meter data, the measurements were converted to absolute units (macroscopic cross sections in units of cm^{-1}) by comparison with the scattering from a calibrated secondary standard consisting of neutron irradiation induced voids in an Al single crystal[22] (denoted as Al-4). Because the relatively large void size ($R_g \sim 210\text{Å}$) in the secondary standard made the Guinier region inaccessible for this instrumental configuration, it was not possible to use the same procedure for converting the 2-meter data into absolute units. Rather, where needed, the two-meter data were scaled by matching with the 10.8 meter data in the region of overlap.

The methods of analyzing these data will be indicated in the following section.

V. Results and Discussion

Measurements were made with sample-detector distances of 18.9, 10.8 and 2.0 meters, as discussed in the previous section. These measurements correspond to observations in q-space in the ranges $0.0028\text{-}0.022\text{Å}^{-1}$, $0.0049\text{-}0.039\text{Å}^{-1}$ and $0.026\text{-}0.21\text{Å}^{-1}$, respectively. The scattering profiles measured with the two longer sample-detector distances were isotropic and very intense in the lower q-region. A representative example of these profiles, after correcting as indicated in the previous section and after radially averaging, is shown in

the form of a log-log plot in Fig. 2a; this is for heat 280 (38 volume per cent ferrite, Table 1) annealed 70,000 hours at 400°C (Table 2). After subtracting the constant background according to the method of Naudon and Caisso[23], the slope in the tail region is found to be -3.9_4 as indicated in the figure. This value is in excellent agreement with the expected theoretical value of -4 from the Porod law[17], eq. 6. A Guinier plot of these same data is shown in Fig. 2b. The slope in the linear, low-q region indicated in the figure yields, according to eq. 5, an apparent Guinier radius of 566 Å. This observation is fairly typical of the low-q results for the entire matrix of samples listed in Table 2, irrespective of the ferrite content of the alloy or of the heat treatment. Measurements made with a 4 kilogauss magnetic field applied showed that this region of the small angle neutron scattering profile is dominated by magnetic scattering. No precipitates of such size and volume fraction are known to exist in these duplex steels. Hence, to the extent that our SANS measurements extend to sufficiently low q to allow the full Guinier region to be sampled, this apparent particle size of some 1500Å diameter should most probably be interpreted as a measure of the size of the magnetic domains in the ferrite phase. Note, however, that the present experiment has only established that this component of the scattering is magnetic in origin. It cannot be ruled out that the intense low-q scattering is due to some other process, such as refraction[24] associated with magnetic domains. Additional research to elucidate the nature of the magnetic inhomogeneities is needed. To a large extent, the 10.8 meter data were quite similar, and, since our primary interest was with the small chemical precipitates, the analysis and discussion to follow will deal mostly with the 2 meter data.

Figure 3a presents a log-log plot of the 2 meter scattering from SS#3 (heat 278 annealed 70,000 hours at 400°C) and SS#4 (heat 280 annealed 66,650 hours at 400°C). Except for a scaling factor, which will be discussed presently, the similarity of these two scattering curves is striking. The broad maxima in these profiles shift toward lower q-values with continued annealing and signify a non-random spatial distribution of precipitate particles. This feature has been noted to a greater or lesser extent in all the 2 meter profiles measured (see Table 2), which suggests non-random nucleation of the precipitates. This should not be misinterpreted as evidence for heterogeneous nucleation at defects, such as dislocations. Rather, it is more likely the result of elastic interactions which have influenced the choice of nucleation sites, or simply the high density of scattering centers.

A more or less conventional Guinier analysis of these data yields mean spherical particle diameters* of 74 and 70 Å for samples SS#3 and SS#4, respectively. Based on the literature results summarized in a previous section, these particles are surely what Chopra and Ayrault[9] have termed "$M_{23}C_6$-like", which they have shown to be on the order of 50 Å in diameter and to be enriched in nickel and silicon. This points out a shortcoming of small angle scattering in cases where more than one type of defect may be present. That is, the method yields the weighted sum of the scattering from all defects present in the scattering volume, and, except in special cases such as contrast matching or isotopic enrichment, there is no *a priori* means of knowing which type of defect is giving the observed scattering. On the other

*The Guinier analysis tends to overestimate the particle size as will be discussed later.

hand, for a typical SANS experiment one may sample the scattering from 10^{15}-10^{18} particles; hence, the result is inherently statistically representative of the bulk material.

The striking similarity of the two scattering curves in Fig. 3a was not unexpected. Provided there is no change in the decomposition mechanism or a change in the morphology of the daughter phase, according to the scaling law proposed by Furukawa,[25] the small angle scattering spectra for different decomposition times (t) at a given temperature should scale according to

$$I(q,t) = q_m^{-3}(t)\, F\left(\frac{q}{q_m(t)}\right), \tag{12}$$

where $q_m(t)$ is the q-value corresponding to the peak in the scattering curve. As was pointed out by Forouhi,[26] use can be made of this similarity to infer additional useful information. After applying appropriate magnification factors to the $I(q)$ and q values for the SS#3 data, the scaled results along with the unscaled data for SS#4 are shown in Fig. 3b; the agreement is quite remarkable. It is perhaps worth pointing out that the intensity scaling factor (2.25) is just equal to the ferrite ratio in these two samples (Table 1), within the accuracy to which the latter values are known.

The same procedure has been utilized to scale the SANS data for the relatively short time runs (10,000 hours) at 400°C for comparison with the anneals of about 70,000 hours. The unscaled, radially averaged scattering data for heat 278 (low ferrite content) are shown in Fig. 4a and those for heat 280 (high ferrite content) in Fig. 4b. It was somewhat surprising to find the scattered signal from the higher ferrite alloy (SS#8, Fig. 4b) to be so much weaker than that from the lower ferrite alloy (SS#7, Fig. 4a), each having been annealed 10,000 hours at 400°C. Significantly, Chopra and

Ayrault[9] reported seeing no precipitates in their TEM examination from heat 280 annealed 10,000 hours at 400°C. Although it is not readily apparent from the lower curve in Fig. 4b, the scattering from SS#8 is significantly above zero. After scaling the SS#8 data with that from SS#4, it is estimated that the precipitates in heat 280 after annealing 10,000 hours at 400°C are about 26 Å in diameter; however, the volume fraction is not known. Similarly, the precipitates in the low ferrite steel annealed for the same time and temperature are estimated to be about 41 Å in diameter. This scaling procedure has been used for the ten conditions of composition, annealing temperature and annealing time examined, and a summary of the particle sizes so derived is given in the last column of Table 2. The scattering from heat 280 annealed 3000 hours at 300°C was too weak to yield a mean particle size estimate. It is regrettable that no unaged specimens of these two steels were available for direct comparison with SS#10. While it may be remarked that these particles are quite small, it should be realized that an iron particle 20Å in diameter contains some 350 atoms. Hence a substantial amount of clustering has occurred even in the steels where the smallest particles were found. While it is not possible from the limited matrix of the present experiment to discern the detailed mechanism which yielded these small agglomerates, the cluster coagulation mechanism put forth by Binder[27] would appear to be highly plausible. Such a rapid "decomposition" was observed in a binary Ni-Al alloy by Epperson and Fürnrohr,[28] and the changes occurring[29] in this latter system during the "incubation period" are almost surely due to the cluster coagulation mechanism described by Binder.

According to various scaling theories[25,27,30,31,32,33], simple power law expressions describe the time dependence of the location in reciprocal space (wave number) of the maximum in the scattering curve

$$q_m(t) \propto t^{-a} \tag{13a}$$

and of the peak intensity

$$I_m(t) \propto t^{b}, \tag{13b}$$

the exact values of a and b depending on the theory. For the low ferrite steel (heat 278) annealed at 400°C, the value of the exponent a is found to be 0.30 and that of b to be 0.72. While our two available data points used to derive these values are clearly insufficient to permit an unqualified statement as to the relevant mechanism operating over the annealing period involved, it is worth noting that the observed value of a is in reasonable agreement with the theoretical value of 1/3 predicted for late stage annealing (coarsening, or ripening) by Lifshitz and Slyozov,[31] Wagner,[30] Binder[27] and Furukawa.[25] This observation must be tempered by the realization that the theoretical ratio of b/a is 3 while the experimental ratio is 2.4. The tentative conclusion that ripening is occurring after some 70,000 hours at 400°C in the low ferrite steel is supported qualitatively, however, by particle size distributions which are considered next.

The integral transform method of Brill and Schmidt[18] (BS) for determing the distribution of particle sizes from small angle scattering data has been described in section III, equations 9-11. This procedure explicitly assumes the particles are spherical and are non-interacting. Only to the extent that these restrictive assumptions are fulfilled by the system being investigated can the results from a Brill-Schmidt particle size analysis be taken

literally.* The particle size distributions, in relative units, determined for the low ferrite steel (heat 278) after annealing 10,000 hours and 70,000 hours at 400°C are shown in Figs. 5a and 5b, respectively. What is particularly noteworthy is the form of the distribution for the long-time aged sample. For an alloy system in the later stages of decomposition, and which fulfills the conditions assumed by BS, the expected form of the particle size distribution is known from the theoretical work by Lifshitz and Slyozov[31] and of Wagner[30] (LSW). A distribution curve generated according to the LSW theory for particles 75 Å in diameter is shown in Fig. 6 and which is characterized by a tail which approaches zero diameter smoothly and by a rather abrupt drop-off on the large particle side of the distribution. The striking difference between the characteristic LSW distribution and that determined for the long-time aged experimental data by the BS method shown in Fig. 5b is obvious. However, if one simulates intensity data for an assemblage of particles distributed according to the LSW theory and then processes these simulated SAS data according to the BS procedure, one recovers[34] a size distribution curve very much like that shown in Fig. 5b rather than that in Fig. 6. It is beyond the intended scope of this discussion to explore why such a discrepancy should exist. Rather, on the basis of simulations along the lines mentioned above, it is asserted that the experimental distribution shown in Fig. 5b supports the contention that after 70,000 hours at 400°C the low ferrite steel is undergoing Ostwald ripening. A similar particle size distribution is obtained for the higher ferrite duplex stainless steel, and it appears that it too is probably undergoing coarsening after some 66,650 hours

*If one were to be completely inflexible in requiring fulfillment of all inherent assumptions in the relevant small angle scattering theories, one would rarely be able to proceed, even to the extent of determining a Guinier radius in a metallic alloy.

at 400°C. On the other hand, the size distribution obtained for heat 278 after 10,000 hours at 400°C (Fig. 5a) is more "normal". This may indicate that nucleation is not yet complete after the shorter annealing period and hence may account for the experimental power law coefficients not agreeing more closely with theory. Given the importance of understanding the detailed annealing behavior of this class of duplex stainless steels and the ease of application of such small angle scattering techniques as those related above, it would appear worthwhile to investigate a more complete annealing sequence of duplex steels. Furthermore, it must be emphasized again that the explicit assumptions embedded in the Brill-Schmidt procedure are not fulfilled for this alloy; consequently, the resulting particle size distributions should not be accepted literally.

As indicated in section IV, a few crucial measurements were made with the sample immersed in an external magnetic field, as an aid in establishing the origin of the observed small angle neutron scattering. This results in an anisotropic two-dimensional scattering pattern as shown in Fig. 7a for the 2-meter data from SS#3 (heat 278) annealed 70,000 hours at 400°C. A section through this pattern where the scattering vector is parallel to the magnetic field direction is shown in Fig. 7b, and a similar cut for the case when these two vectors are perpendicular is presented in Fig. 7c. The relationship expressed by equation 1 permits separation of the nuclear and magnetic scattering and hence allows these components to be analyzed separately.

After completing the experimental scattering measurements, it was a pleasant surprise to learn that the composition of the precipitates in a CF8 steel had been determined recently by field ion microscopy by Miller, Bentley,

Brenner and Spitznagel.[35]* However, the detailed composition of the ferrite matrix, after decomposition at the relevant temperatures, is not known.[36] In order to calculate the difference in scattering length density ($\Delta\rho$) in equations 7 and 8, one must know the concentration of the matrix as well as that of the embedded precipitates. This had the immediate consequence of preventing our using expression 7 to estimate the number density of precipitate particles and expression 8 to determine their volume fraction. It is perhaps worth digressing to note that for a binary alloy, the method of Gerold[37] permits the concentrations of the coexisting daughter and parent phase to be determined from SAS analysis. At least one attempt has been made in a ternary alloy[38], with only modest success. In a system as complex as a commercial grade steel, an extension of these methods would appear not to be feasible at present. For the more rigorous SAS analysis to proceed in complex alloy systems, such concentration information must be known from other sources.

It is possible, nevertheless, in the present case to make an estimate of the volume fraction of precipitate in the ferrite phase from information at hand. The peak in the scattering curve (e.g., Fig. 4a) yields a crude estimate of the mean inter-precipitate distance ($\bar{d}$), and a mean particle radius ($\bar{r}$) can be obtained from the particle size distributions (e.g., Fig. 5b). Hence,

$$f_v \cong 8\left(\frac{\bar{r}}{\bar{d}}\right)^3 . \qquad (14)$$

*Miller, Bentley, Brenner and Spitznagel[35] report the following composition of the precipitates. in wt %, with probable errors (2σ)

Si	Ni	Fe	Mo	Cr	C
14.9±1.8	27.0±3.6	22.0±3.3	23.9±4.6	12.0±2.5	0.23±0.16

For heats 278 and 280 annealed for the longest times at 400°C (Table 2), the precipitate volume fractions in the ferrite phase are estimated to be 18 and 12%, respectively, using one cm^3 of material as the basis and the relationship

$$N_p \overline{V}_p = f_v \quad . \tag{15}$$

This translates to a number density of particles of on the order of 10^{18} per cm^3. It should be emphasized that the Guinier radius does not yield a particle size dimension suitable for use in eq. 14. When a distribution of particles is present in the sample, as is usually the case, the scattering tends to be dominated by the larger particles, and hence the Guinier radius, likewise, tends to overestimate the mean particle size. Due to the recognized crudeness of the volume fraction estimates and the potential for confusion or misuse, values of f_v are not presented for the remaining heat treatments. Rather, it is suggested that a more comprehensive SANS determination be carried out along the lines indicated earlier, once the composition of the ferrite matrix is known at the appropriate temperatures.

Because different experimental conditions were used, a rigorous comparison with the volume fraction and mean number density of particles cannot be made with the values recently found by field ion microscopy by Miller, et al.[35]; however, the present results appear to be consistent with their values of about 10^{17} particles/cm^3 with a volume fraction of 0.05 in a CF8 alloy annealed 7500 hours at 400°C.

VI. Summarizing Conclusions

In this investigation, the small angle neutron scattering from two cast duplex stainless steels aged for times from 3,000 hours to 70,000 hours was studied in the range from $0.0028 \lesssim q \lesssim 0.2 \text{Å}^{-1}$. In the lowest q region, the scattering was dominated by magnetic scattering effects associated with the ferrite phase. The scattering in the low q region was not exclusively magnetic in origin; however, this non-magnetic scattering was not investigated systematically because of limited time on the SANS instrument.

The scattering in the higher-q region was reasonably intense and revealed a volume fraction of precipitate, in the ferrite, estimated to be 12-18 volume percent after long time aging. This precipitate is the Ni and Si rich phase discussed by Chopra and Ayrault[9] for which the composition was recently determined by field ion microscopy by Miller, Bentley, Brenner and Spitznagel.[35] After 70,000 hours at 400°C, it was estimated that there were on the order of 10^{18} precipitate particles per cm^3 of ferrite and that these particles were on the order of 50 Å in mean diameter. These particles were distributed in a non-random manner; that is, spatially, short-range-ordered. In addition, this investigation suggests that after 70,000 hours aging at 400°C the precipitate in the ferrite phase is undergoing Ostwald ripening. It is presently unclear after what time the nucleation is complete. It would be feasible and useful, particularly with respect to determining the mode of decomposition, to investigate more extensively the kinetics of phase separation for times up to at least about 20,000 hours. In the two duplex stainless steels differing in ferrite content by a factor of two, there was an apparent discrepancy in the nucleation and/or growth rate, observed by both TEM and SANS. In any kinetics investigation, both steels should be included in order

to clarify this point.

The matrix of composition/heat treatments investigated here was too small to permit final, comprehensive conclusions to be drawn. Nonetheless, it has been demonstrated that current instruments and analysis techniques are capable of yielding additional, useful information about these practical alloys.

Acknowledgements

One of us (J.E.E.) wishes to acknowledge with gratitude several helpful discussions with Drs. J. B. Darby, Jr., G. Ayrault, H. M. Chung and O. K. Chopra.

References

(1). H. D. Solomon and T. M. Devine in MiCon 78: Optimization of Processing, Properties and Service Performance Through Microstructure Control; eds., H. Abrams, G. N. Manair, D. A. Nail and H. D. Solomon, ASTM STP 672 (1979), 430-461.

(2). P. J. Grobner, Met. Trans. 4 (1973), 251-260.

(3). E. I. Laderman and W. H. Bamford, ASME MPC-8 (1978), 99-128.

(4). R. O. Williams and H. W. Paxton, J. Iron. Steel Inst. 185 (1957), 358-374.

(5). R. O. Williams, Trans. AIME 212 (1958), 497-502.

(6). R. M. Fisher, E. J. Dulis and K. G. Carroll, Trans. AIME 197 (1953), 690-695.

(7). M. J. Marcinkowski, R. M. Fisher and A. Szirmae, Trans. AIME 230 (1964), 676-689.

(8). A. Trautwein and W. Gysel in Stainless Steel Castings; eds., V. G. Behal and A. S. Melilli, ASTM STP 756 (1982), 165-189.

(9). O. K. Chopra and G. Ayrault, NUREG/CR 3857 - ANL-84-44 (1984).

(10). O. K. Chopra and H. M. Chung, in NUREG/CR-3998 Vol. I - ANL-84-60 Vol. I (1984).

(11). G. T. Brown and R. T. Allsop, J. Iron Steel Inst. 194 (1960), 435-442.

(12). H. M. Chung, private communication.

(13). J. B. Darby, Jr., private communication.

(14). G. E. Bacon, Neutron Diffraction, Clarendon Press, Oxford (1975), 21-64.

(15). M. Ernst, J. Schelten and W. Schmatz, phys. stat. sol. (a) 7 (1971), 469-476.

(16). A. Guinier and G. Fournet, Small Angle Scattering of X-rays, John Wiley and Sons, New York (1955).

(17). G. Porod, Z. Kolloid 124 (1951), 83-114; 125 (1952), 51-57 and 108-122.

(18). O. L. Brill and P. W. Schmidt, J. Appl. Phys. 39 (1968), 2274-2281.

(19). J. E. Epperson, B. A. Loomis and J. S. Lin, J. Nucl. Mater. 108-109 (1982), 476-484.

(20). W. C. Koeller, R. W. Hendricks, H. R. Child, S. P. King, J. S. Lin and G. D. Wignall in Scattering Techniques Applied to Supra - Molecular and Non - Equilibrium Systems, eds. S. H. Chen, B. Chu and R. Nossal, Plenum Press, N.Y. (1981) 75-85.

(21). C. J. Borkowski and M. K. Kopp, J. Appl. Cryst. 11 (1978), 430-434.

(22). R. W. Hendricks, J. Schelten and W. Schmatz, Phil Mag 30 (1974), 819-837.

(23). A. Naudon and J. Caisso, J. Appl. Cryst. 7 (1974), 25-36.

(24). N. F. Berk and K. Hardman-Rhyne, submitted to J. Appl. Cryst.

(25). H. Furukawa, Phys. Rev. A23 (1981), 1535-1545.

(26). A. R. Forouhi, Kinetics of Phase Separation and Coarsening in Al-22 at. % Zn-0.1 at. % Mg, PhD dissertation, University of California at Berkeley (1982).

(27). K. Binder, Phys. Rev. B15 (1977), 4425-4447.

(28). J. E. Epperson and P. Fürnrohr, Acta Cryst. A39 (1983), 740-746.

(29). J. E. Epperson and J. S. Lin, research not yet published.

(30). C. Wagner, Z. Electrochem 65 (1961), 581-591.

(31). I. M. Lifshitz and V. V. Slyozov, J. Phys. Chem. Solids 19 (1961), 35-50.

(32). K. Binder and D. Stauffer, Phys. Rev. Lett. 33 (1974), 1006-1009.

(33). J. S. Langer, M. Bar-on and H. D. Miller, Phys. Rev. A11 (1975), 1417-1429.

(34). J. E. Epperson, unpublished research.

(35). H. M. Miller, J. Bentley, S. S. Brenner and J. A. Spitznagel, Journal de Physique, in press.

(36). O. K. Chopra, private communication.

(37). V. Gerold, phys. stat. solidi 1 (1961), 37-49.

(38). V. Gerold, J. E. Epperson and G. Kostorz, J. Appl. Cryst. 10 (1979), 28-33.

Table 1. Chemical Compositions of the Two CF-8 Grade Steels[a] Used in the SANS Investigation[9]

Heat	Composition, Wt%										Ferrite content, %	
	Mn	Si	Mo	Cr	Ni	P	S	N	C	Fe (balance)	calc	meas
278	0.28	1.00	0.13	20.20	8.27	0.008	0.019	0.027	0.038	70.0	19.00	15
280	0.50	1.37	0.25	21.60	8.00	0.015	0.006	0.029	0.028	68.2	38.7	38

[a]Obtained from George Fischer, Ltd., Schaffhausen, Switzerland.

Table 2. Summary of the Annealing Schedules of the Samples Investigated[a]

Sample Designation		T_a(°C)	t_a(hrs)	$\bar{D}$(Å) $\bar{D}=2\sqrt{5/3}\,R_g$
278C8	(SS#3)	400	70,000	73.8
280A8	(SS#4)	400	66,650	70.2
278C8	(SS#7)	400	10,000	40.8
280C8	(SS#8)	400	10,000	26.1
278B8	(SS#5)	350	70,000	20.1
280B8	(SS#6)	350	70,000	29.7
278A8	(SS#1)	300	70,000	29.4
280C8	(SS#2)	300	70,000	21.4
278A6	(SS#9)	300	10,000	22.7
280A5	(SS#10)	300	3,000	----

[a] Samples obtained from George Fischer, Ltd., Schaffhausen, Switzerland, by way of J. B. Darby, Jr.[13]

Figure Captions

Fig. 1. Time-temperature diagram for formation of various phases at temperatures above 400°C in cast duplex stainless steel after Solomon and Devine[1].

Fig. 2. (a) Log-log plot of the absolute, total small angle scattering measured at 18.9 meters for the 38 percent ferrite stainless steel annealed 70,000 hours at 400°C.

(b) Guinier plot of these same data. Mean Guinier radius is 556Å.

Fig. 3. Small angle neutron scattering from SS#3 and SS#4. See Table 2 for annealing schedule.

(a) log-log plot showing the similarity of these two scattering profiles.

(b) I(q) vs q after scaling the data for SS#3. See text for more details (f_x = 1.06 and f_y = 2.25).

Fig. 4. Scaling of the 2 meter SANS data for the 10,000 hour anneal at 400°C with that for about 70,000 hours.

(a) heat 278, 15 percent ferrite

(b) heat 280, 38 percent ferrite

Fig. 5. Distribution of particle sizes determination according to the Brill-Schmidt technique for heat 278 annealed; (a) 10,000 hours at 400°C and (b) 70,000 hours at 400°C. Note these data are in relative units; that is, the number of particles of a given diameter per unit volume. These data are normalized such that the most populous value of $\rho(D)$ is assigned the value of unity.

Fig. 6. Particle size distribution for a mean particle diameter of 75Å, generated according to the LSW theory.

Fig. 7. Scattering measured at a sample-detector distance of 2-meters in an external magnetic field of 4 kilogauss for the low ferrite steel annealed 70,000 hours at 400°C.

(a) Isointensity contour diagram

(b) Center cut in the horizontal direction where the scattering vector was parallel to the magnetic field direction.

(c) Vertical cut where the scattering vector was perpendicular to the magnetic field direction.

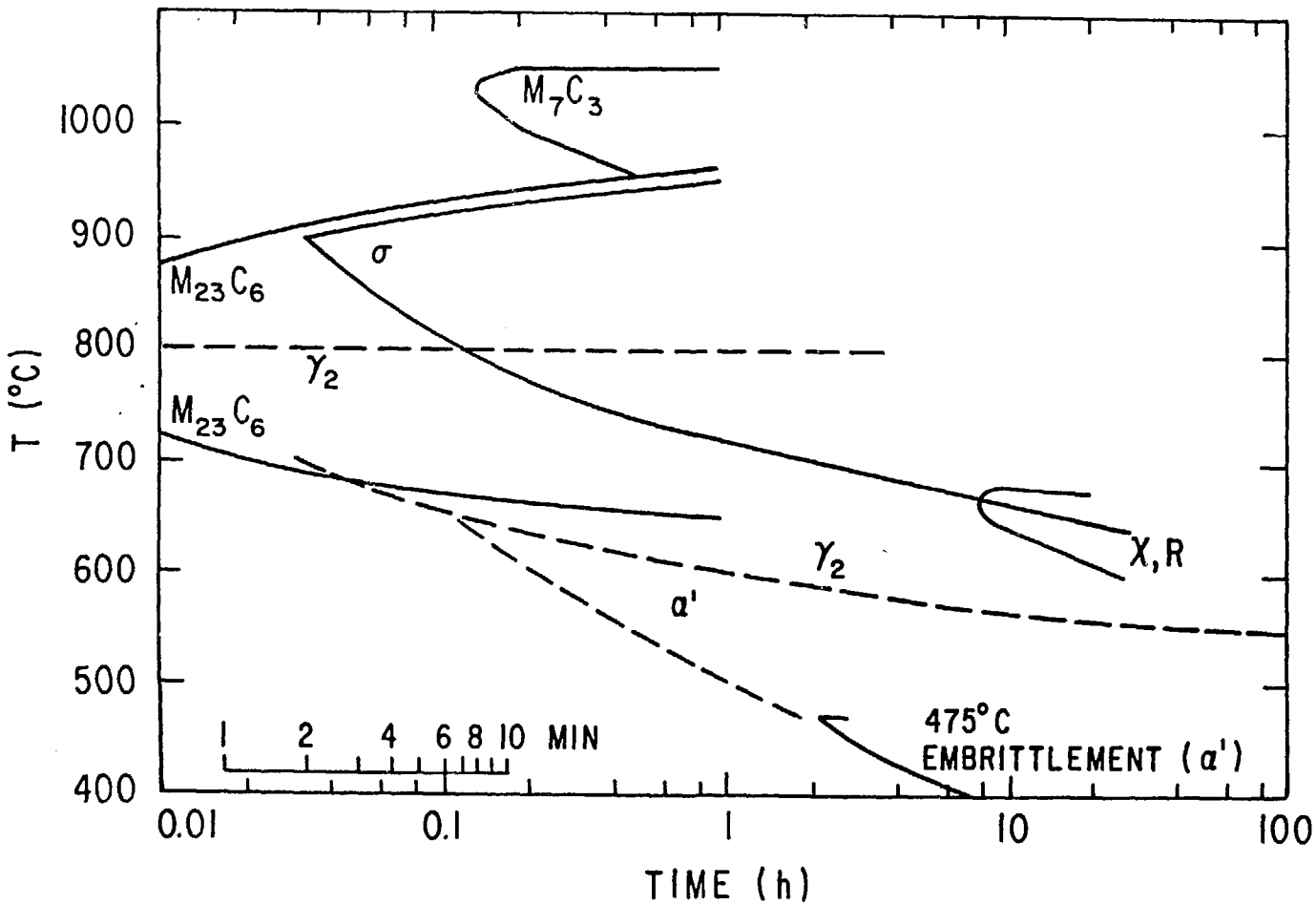
1000
900
800
700
600
500
400
T (°C)
M_7C_3
$M_{23}C_6$
σ
γ_2
$M_{23}C_6$
γ_2
α'
X, R
1 2 4 6 8 10 MIN
475°C
EMBRITTLEMENT (α')
0.01
0.1
1
10
100
TIME (h)

Fig. 1

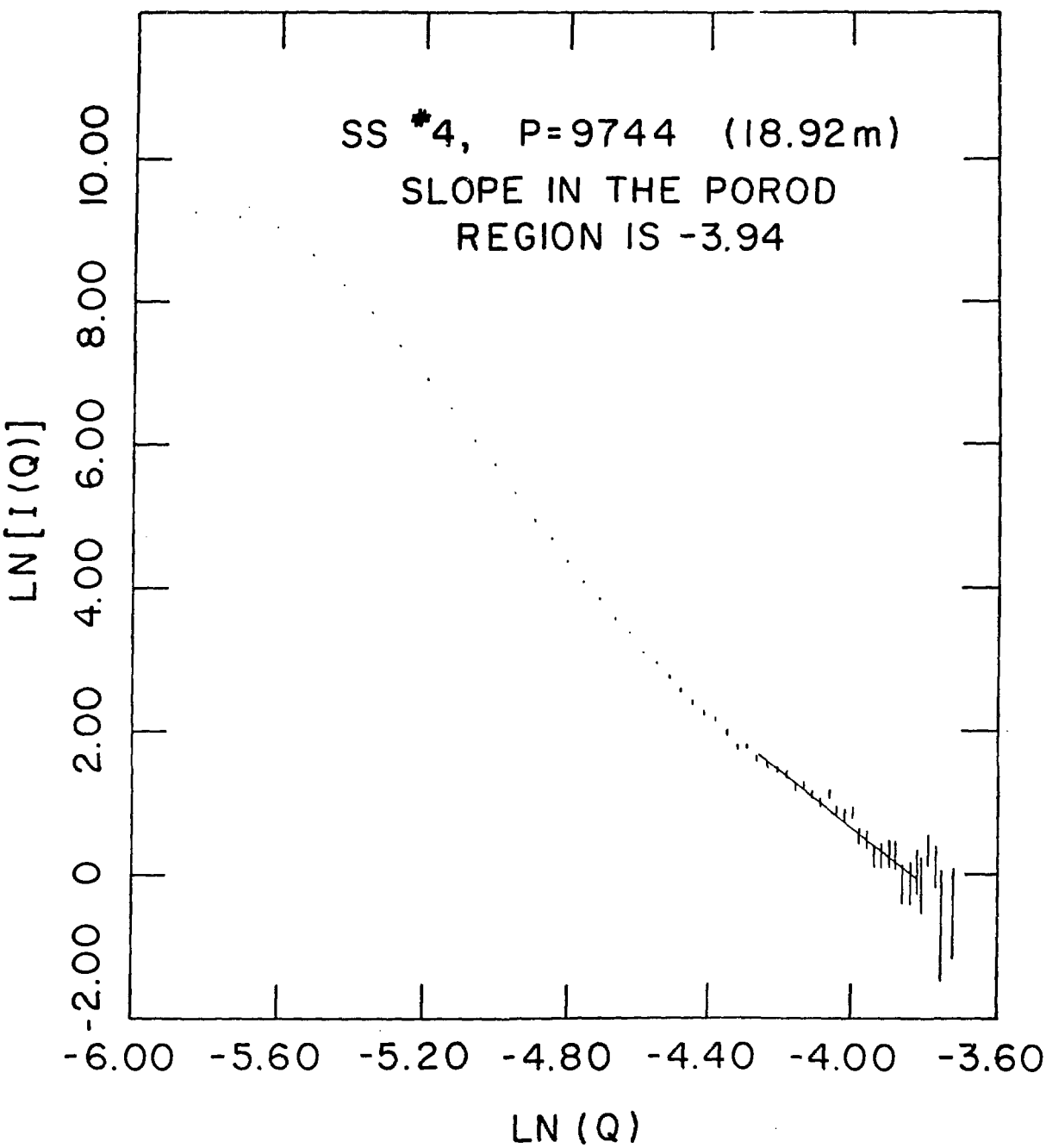
SS #4, P=9744 (18.92m)
SLOPE IN THE POROD
REGION IS -3.94
LN[I(Q)]
10.00
8.00
6.00
4.00
2.00
0
-2.00
-6.00
-5.60
-5.20
-4.80
-4.40
-4.00
-3.60
LN(Q)

Fig. 2a

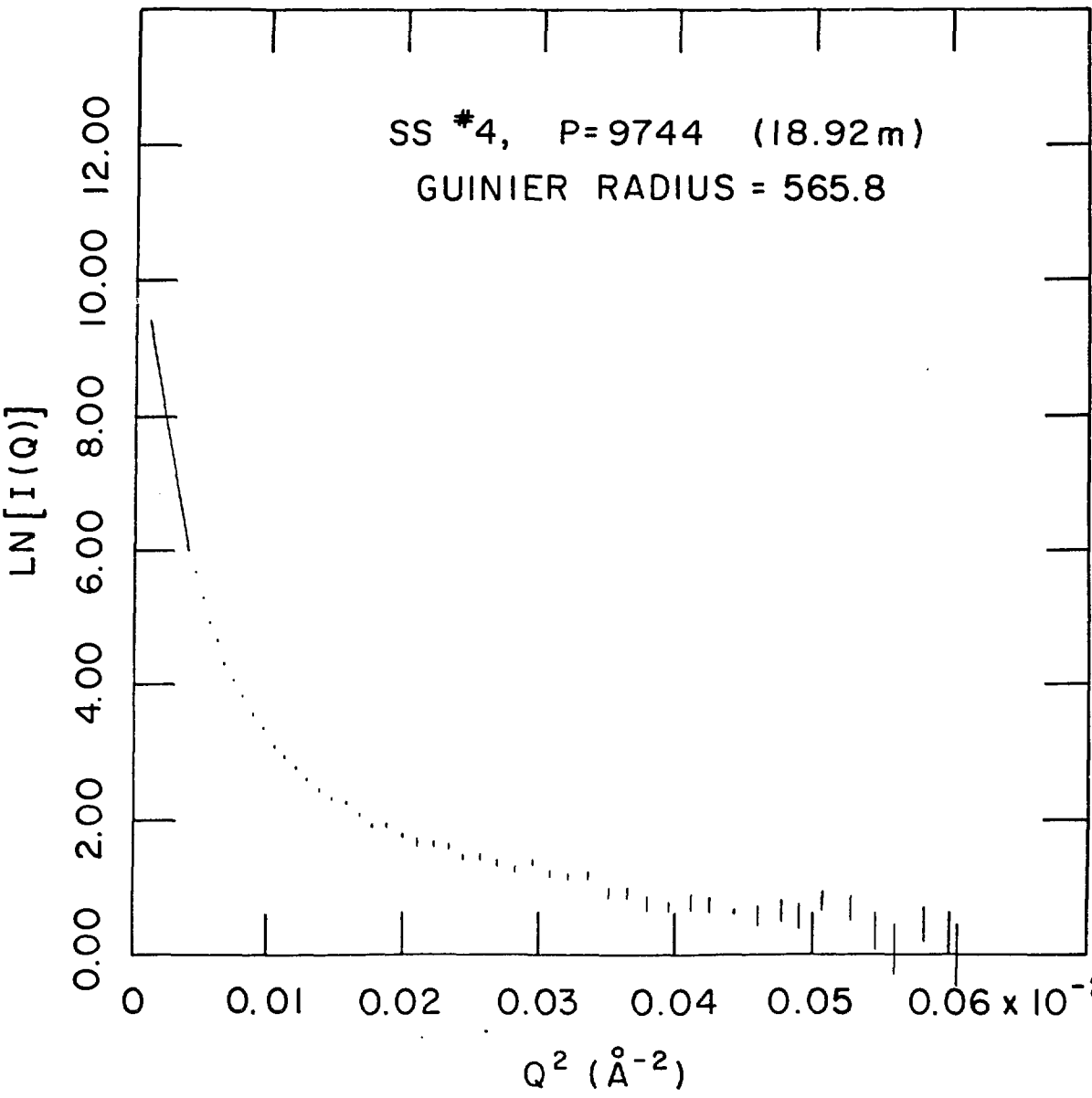
SS #4, P=9744 (18.92m)
GUINIER RADIUS = 565.8
LN[I(Q)]
0.00
2.00
4.00
6.00
8.00
10.00
12.00
0
0.01
0.02
0.03
0.04
0.05
0.06 x 10^-2
Q^2 (Å^-2)

Fig. 2b

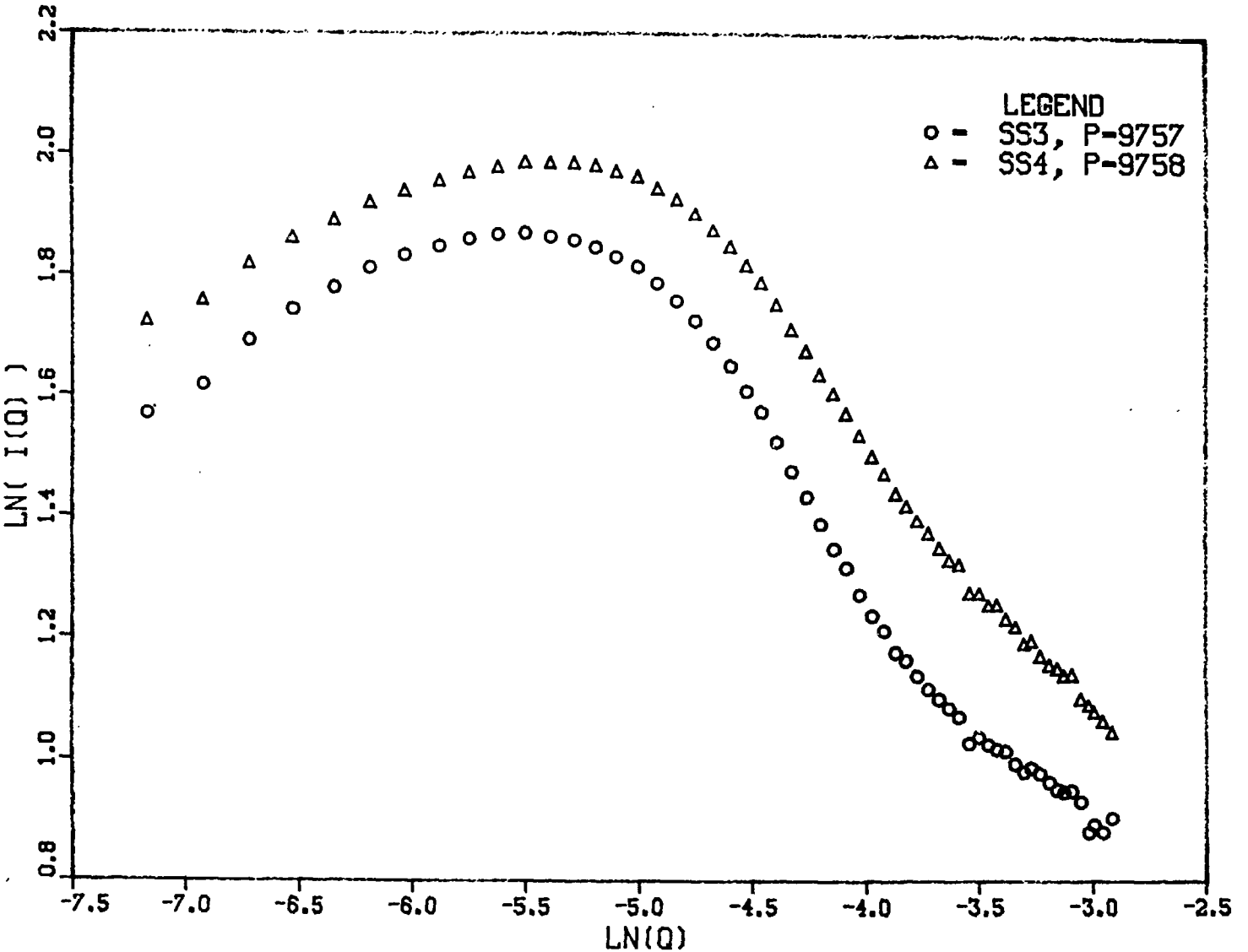
LEGEND
o - SS3, P-9757
Δ - SS4, P-9758
LN(I(Q))
LN(Q)
2.2
2.0
1.8
1.6
1.4
1.2
1.0
0.8
-7.5
-7.0
-6.5
-6.0
-5.5
-5.0
-4.5
-4.0
-3.5
-3.0
-2.5

Fig. 3a

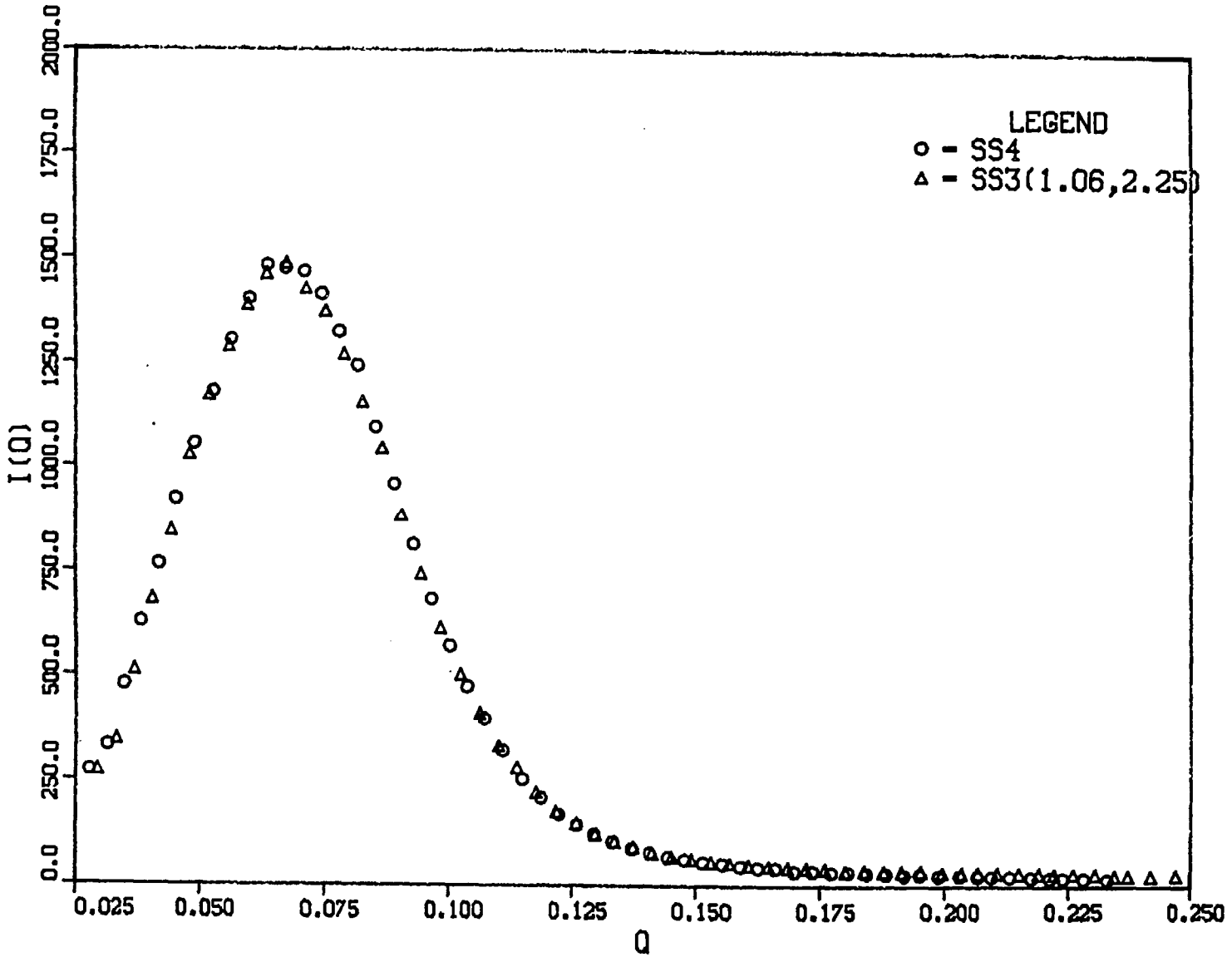
LEGEND
o - SS4
Δ - SS3(1.06,2.25)
I(Q)
Q
0.0
250.0
500.0
750.0
1000.0
1250.0
1500.0
1750.0
2000.0
0.025
0.050
0.075
0.100
0.125
0.150
0.175
0.200
0.225
0.250

Fig. 3b

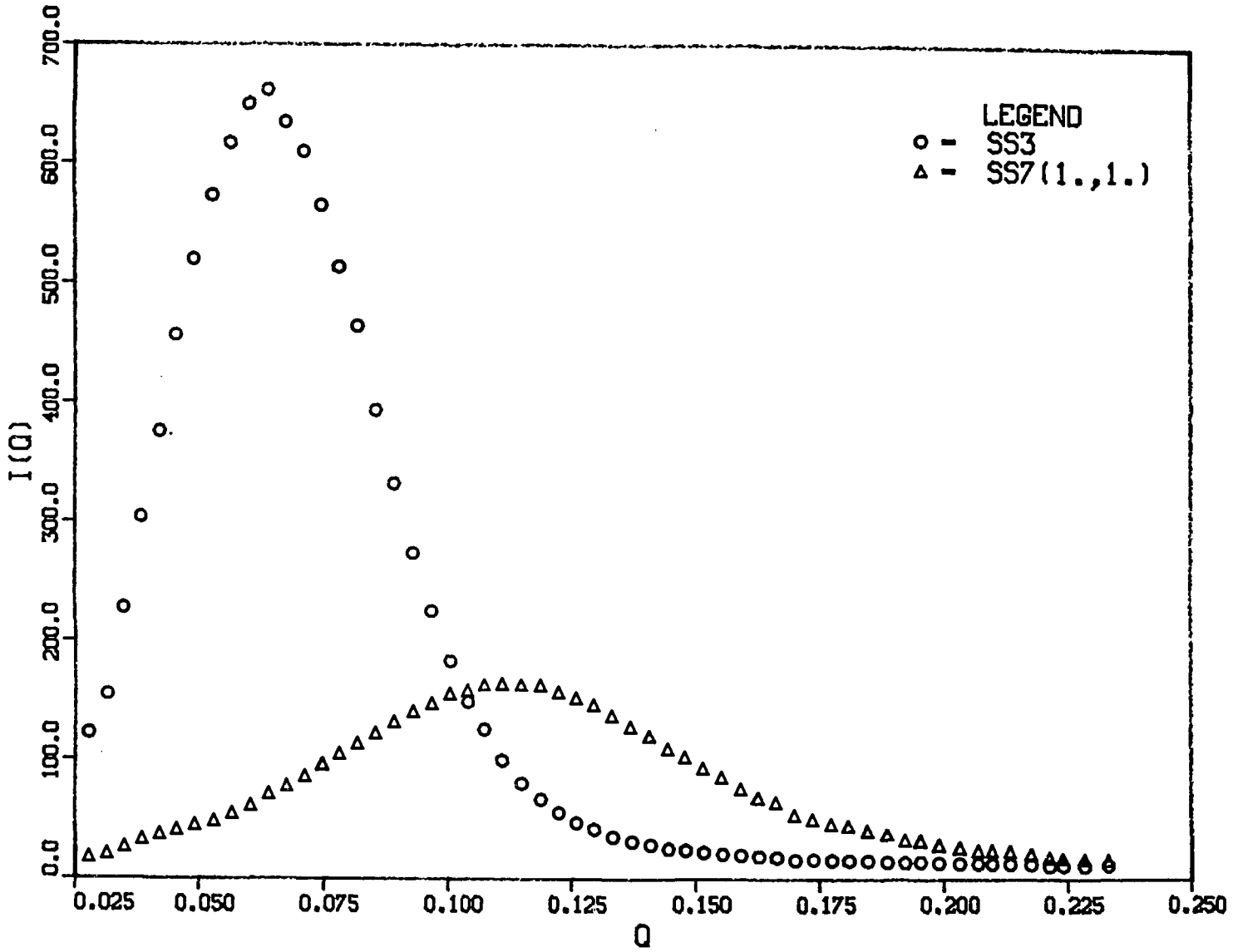
LEGEND
o - SS3
Δ - SS7(1.,1.)
I(Q)
Q
0.0
100.0
200.0
300.0
400.0
500.0
600.0
700.0
0.025
0.050
0.075
0.100
0.125
0.150
0.175
0.200
0.225
0.250

Fig. 4a

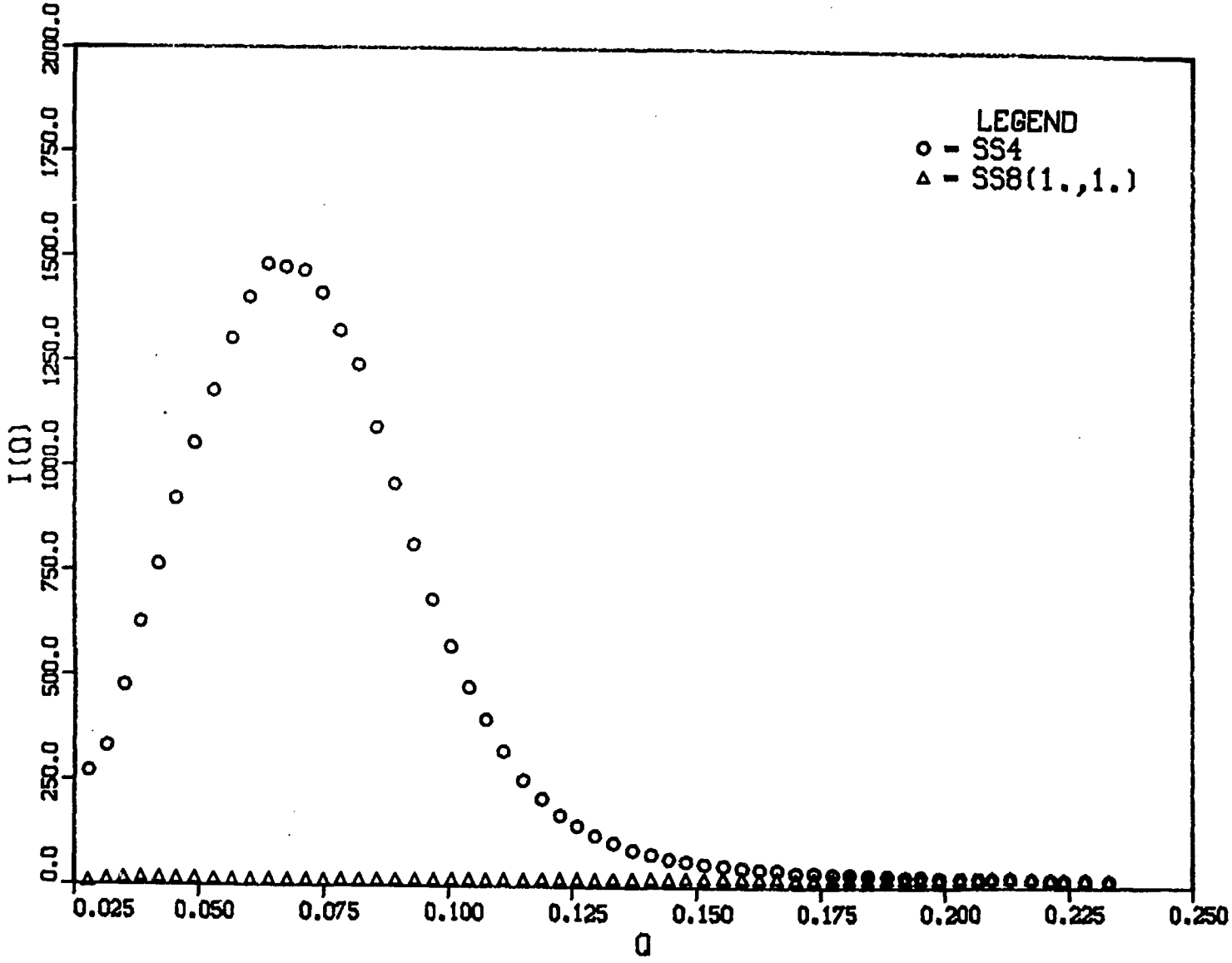
LEGEND
o = SS4
Δ = SS8(1.,1.)
I(Q)
Q
0.0
250.0
500.0
750.0
1000.0
1250.0
1500.0
1750.0
2000.0
0.025
0.050
0.075
0.100
0.125
0.150
0.175
0.200
0.225
0.250

Fig. 4b

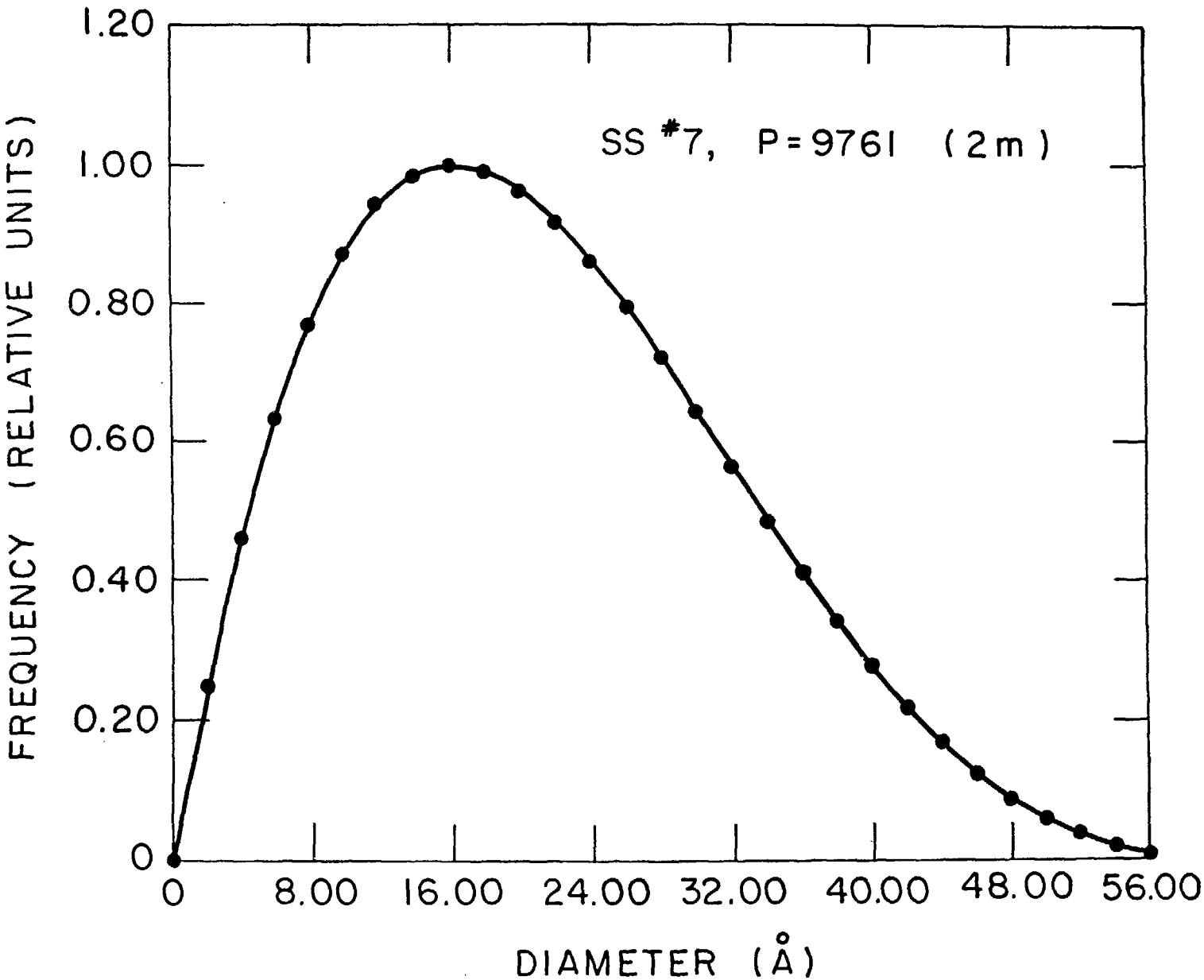
SS #7, P=9761 (2m)
FREQUENCY (RELATIVE UNITS)
1.20
1.00
0.80
0.60
0.40
0.20
0
0
8.00
16.00
24.00
32.00
40.00
48.00
56.00
DIAMETER (Å)

Fig. 5a

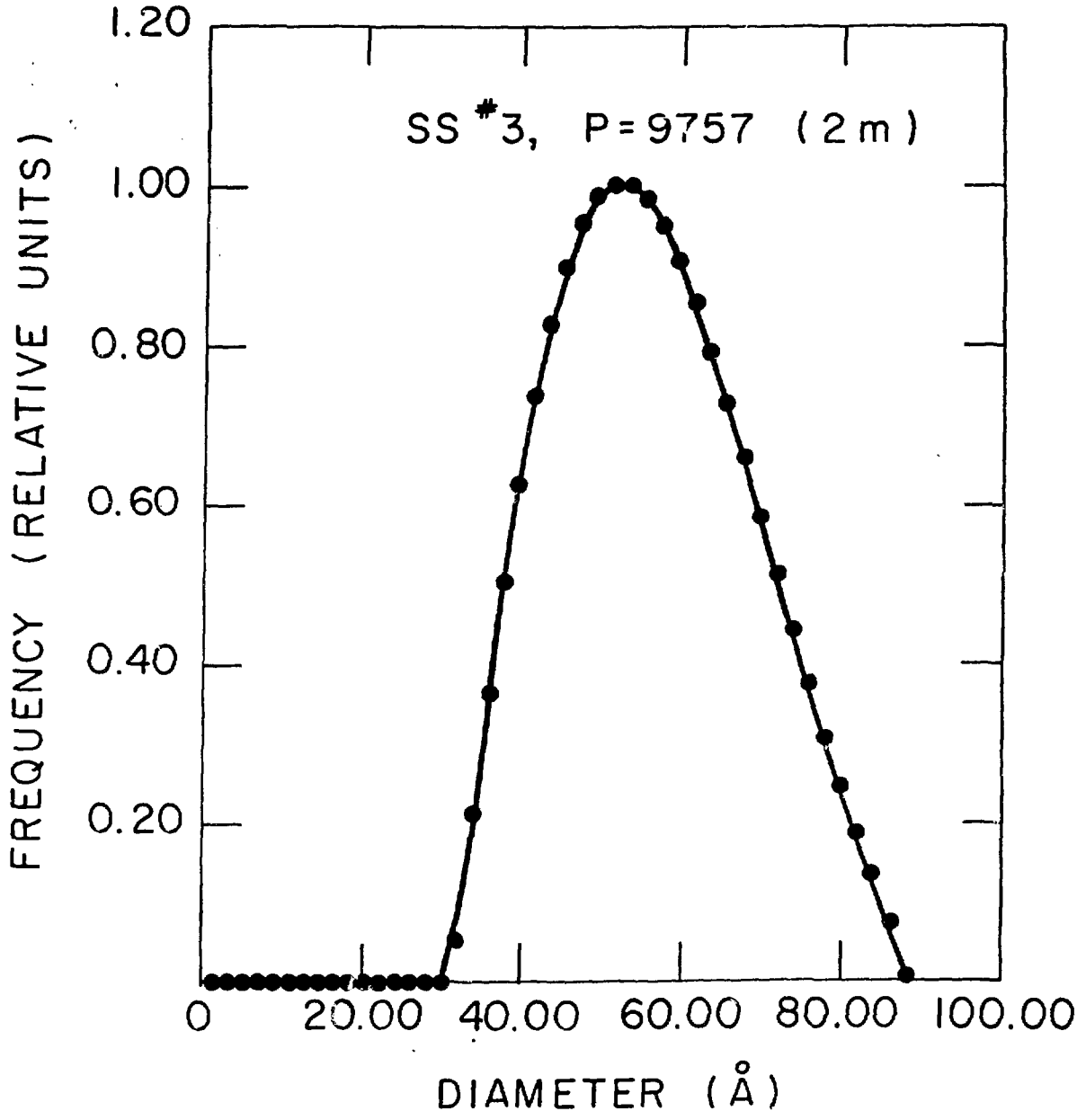
SS #3, P=9757 (2m)
FREQUENCY (RELATIVE UNITS)
1.20
1.00
0.80
0.60
0.40
0.20
0
20.00
40.00
60.00
80.00
100.00
DIAMETER (Å)

Fig. 5b

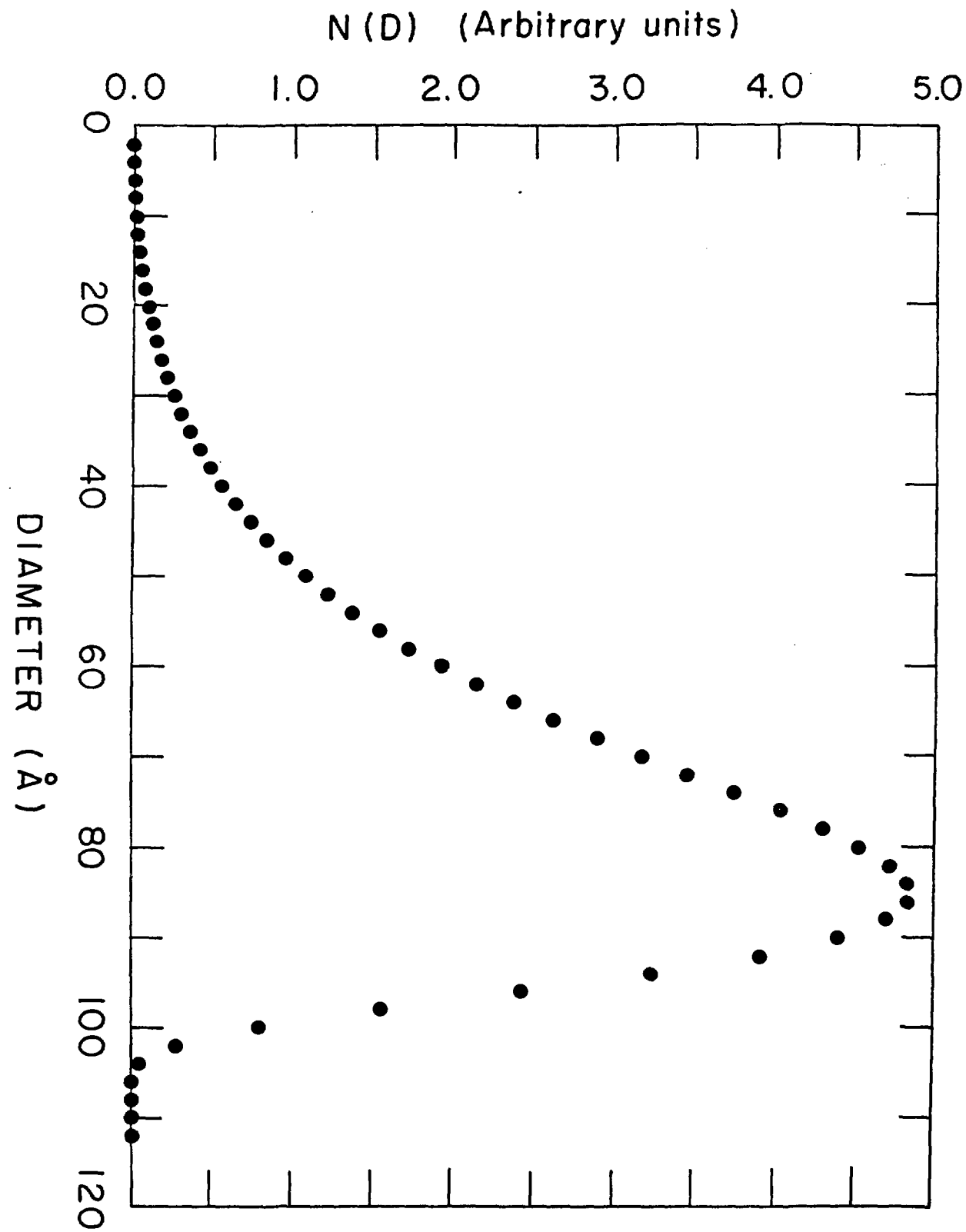
N(D) (Arbitrary units)
0.0
1.0
2.0
3.0
4.0
5.0
0
20
40
60
80
100
120
DIAMETER (Å)

Fig. 6

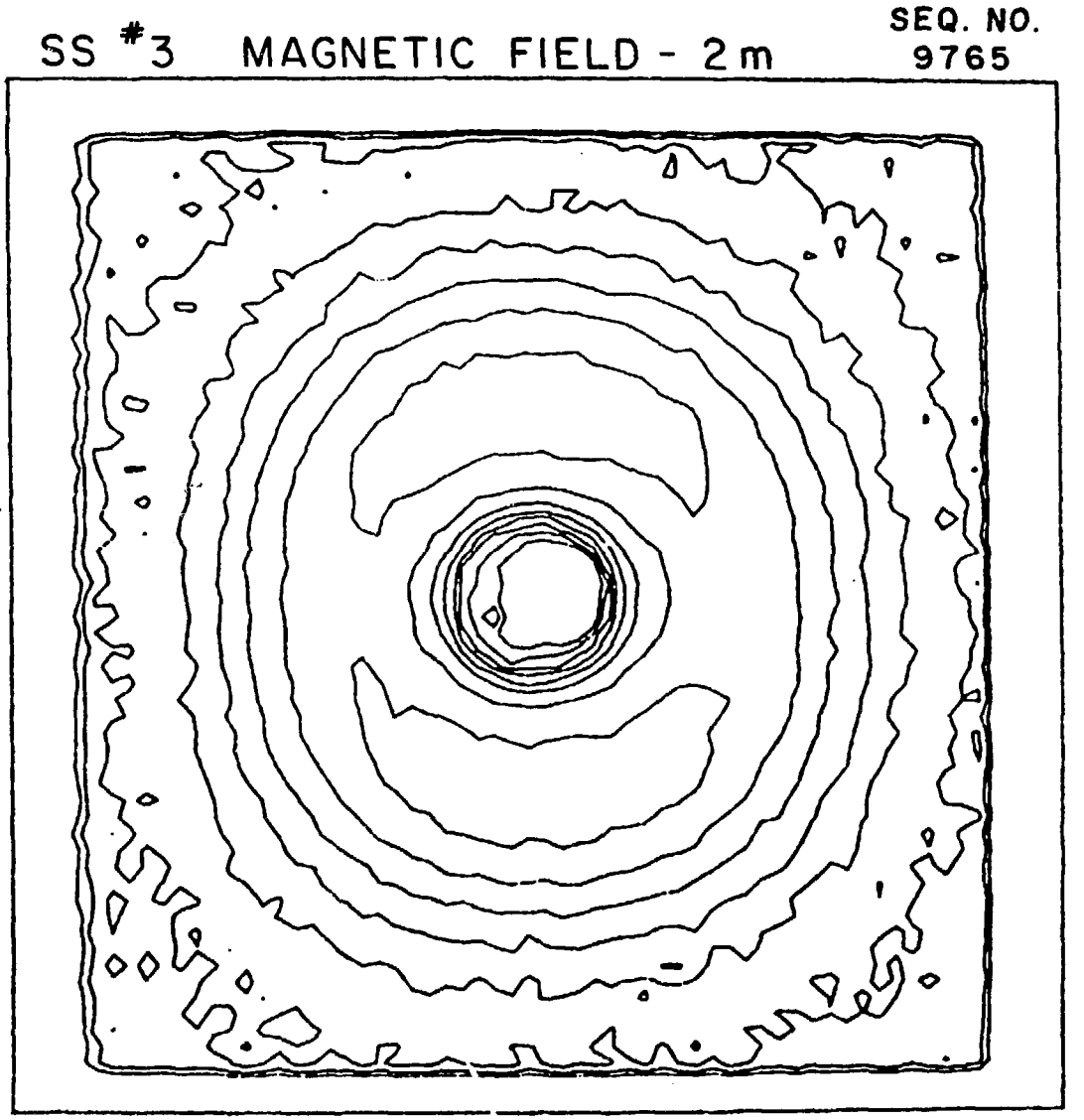

Fig. 7a

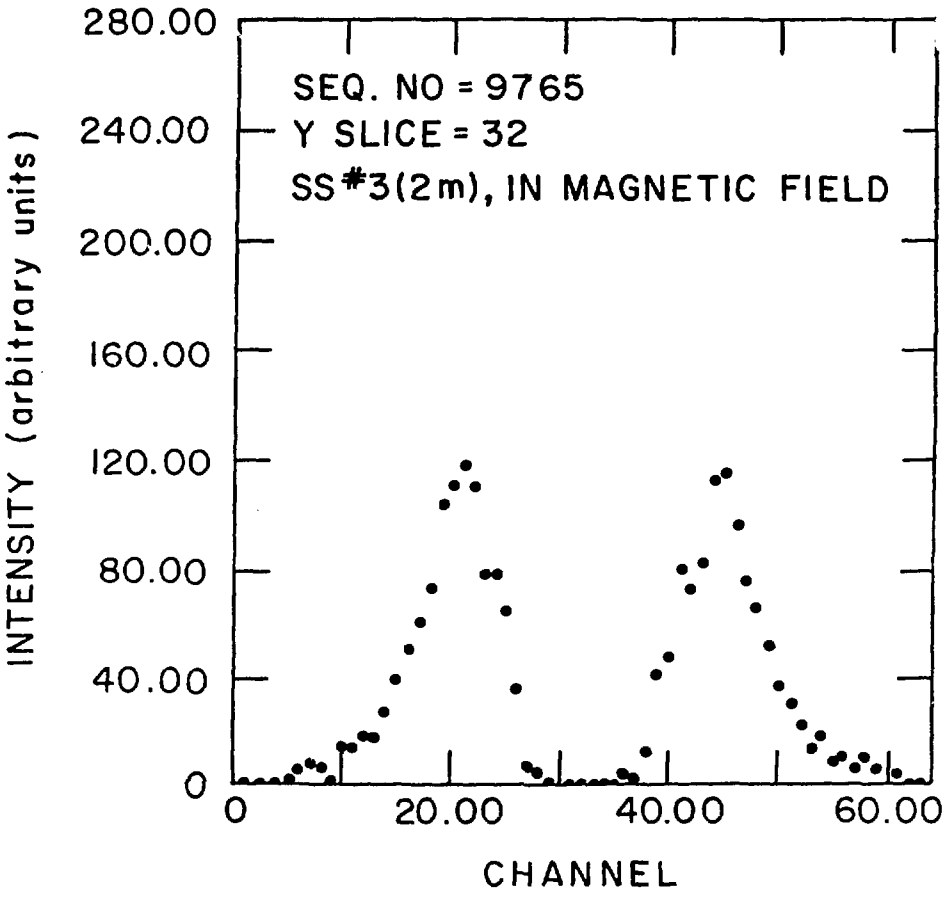
280.00
240.00
200.00
160.00
120.00
80.00
40.00
0
INTENSITY (arbitrary units)
SEQ. NO = 9765
Y SLICE = 32
SS#3(2m), IN MAGNETIC FIELD
0
20.00
40.00
60.00
CHANNEL

Fig. 7b

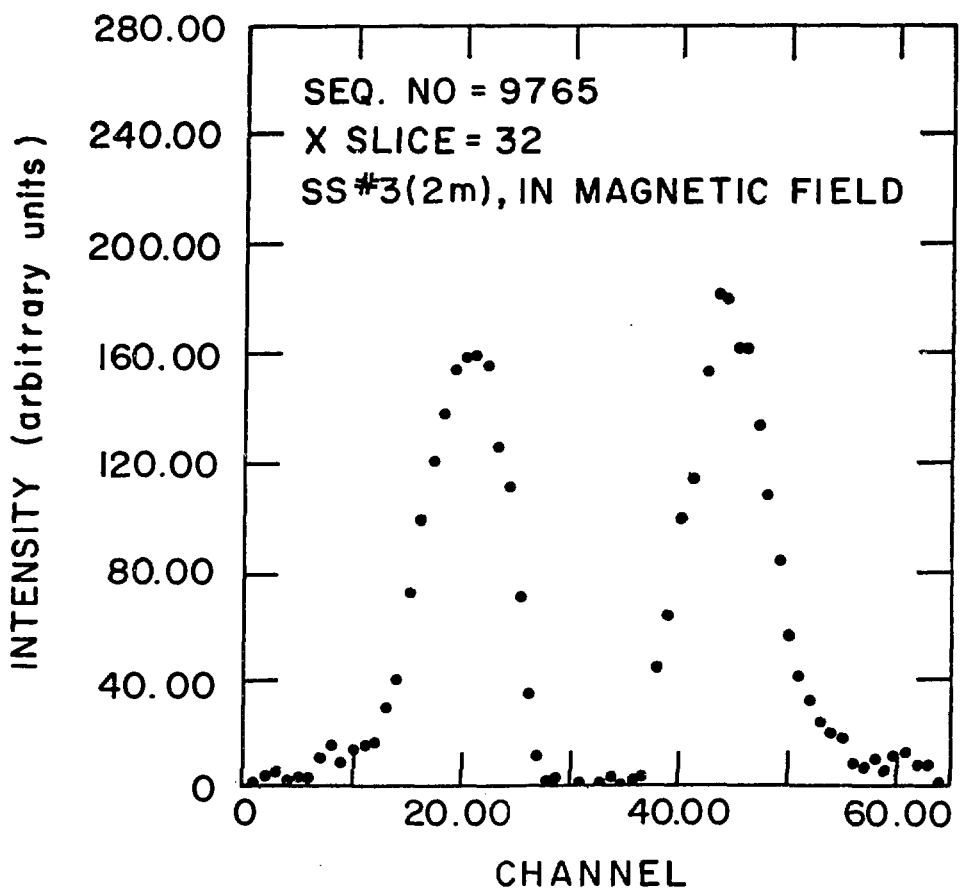
280.00
240.00
200.00
160.00
120.00
80.00
40.00
0
INTENSITY (arbitrary units)
SEQ. NO = 9765
X SLICE = 32
SS#3(2m), IN MAGNETIC FIELD
0
20.00
40.00
60.00
CHANNEL

Fig. 7c